

Theory of perturbation of electrostatic field by an anisotropic dielectric sphere

Akhlesh Lakhtakia

Department of Engineering Science and Mechanics, The Pennsylvania State University, University Park, Pennsylvania 16802, USA

*Nikolaos L. Tsitsas*¹

School of Informatics, Aristotle University of Thessaloniki, Thessaloniki 54124, Greece

Hamad M. Alkhoori

Department of Electrical Engineering, United Arab Emirates University, P.O. Box 15551, Al Ain, UAE

Abstract

The boundary-value problem for the perturbation of an electric potential by a homogeneous anisotropic dielectric sphere in vacuum was formulated. The total potential in the exterior region was expanded in series of radial polynomials and tesseral harmonics, as is standard for the Laplace equation. A bijective transformation of space was carried out to formulate a series representation of the potential in the interior region. Boundary conditions on the spherical surface were enforced to derive a transition matrix that relates the expansion coefficients of the perturbation potential in the exterior region to those of the source potential. Far from the sphere, the perturbation potential decays as the inverse of the distance squared from the center of the sphere, as confirmed numerically.

1 Introduction

When an object made of a certain linear homogeneous dielectric material is exposed to a time-invariant electric field, the atoms constituting the object interact with that electric field until an electrostatic steady state is reached a short time later [1, 2]. This interaction is described in terms of the polarization \mathbf{P} which is the volumetric density of electric dipoles induced inside the object. The polarization \mathbf{P} is linearly proportional of the electric field \mathbf{E} , the proportionality constant being the dielectric susceptibility of the material multiplied by the free-space permittivity. Coulomb's law then leads to the definition of the electric displacement field \mathbf{D} which is linearly related to \mathbf{E} by the permittivity of the material. The permittivity is scalar for isotropic materials but dyadic for anisotropic materials [3, 4].

Perturbation of an electrostatic field by a linear homogeneous dielectric object in free space has been studied for a long time [5–10], presently with biological [11], biomedical [12], electrochemical [13], and manufacturing [14] applications. Let us refer to the electric field present in the absence of the object as the *source field*, the difference between the electric field present at any location outside the object and the source electric field as the *perturbation field*, and the electric field present at any location inside the object as the *internal field*. The boundary-value problem for the electrostatic steady state is solved analytically by (i) expanding the source, perturbation, and internal fields in terms of suitable basis functions and (ii) imposing appropriate boundary conditions at the surface of the perturbing object. The basis functions suitable for representing the source and the perturbation fields are the eigenfunctions of the Laplace equation [5, 15, 16]. When the object is made of an isotropic material, the basis functions suitable for representing the internal field also are the eigenfunctions of the Laplace equation.

¹Corresponding author; e-mail: ntsitsas@csd.auth.gr

Our objective here is to show that analytic basis functions for representing the internal field are available when the perturbing object is composed of an anisotropic dielectric material [17] described by the constitutive relation

$$\mathbf{D}(\mathbf{r}) = \underline{\underline{\varepsilon}} \cdot \mathbf{E}(\mathbf{r}), \quad (1)$$

where the permittivity dyadic

$$\underline{\underline{\varepsilon}} = \varepsilon_0 \varepsilon_r \underline{\underline{A}} \cdot \underline{\underline{A}} \quad (2)$$

involves the diagonal dyadic

$$\underline{\underline{A}} = \alpha_x^{-1} \hat{\mathbf{x}}\hat{\mathbf{x}} + \alpha_y^{-1} \hat{\mathbf{y}}\hat{\mathbf{y}} + \hat{\mathbf{z}}\hat{\mathbf{z}} \quad (3)$$

with ε_0 denoting the permittivity of free space. Any real symmetric dyadic can be written in the form of Eqs. (2) and (3) by virtue of the principal axis theorem [18, 19]. The only conditions imposed by us are that the scalars $\alpha_x > 0$, $\alpha_y > 0$, and $\varepsilon_r > 0$. Natural materials of such kind exist [17]. Materials of this kind can also be realized as homogenized composite materials by properly dispersing dielectric fibers in some host isotropic dielectric material [20].

The positive definiteness [21] of $\underline{\underline{A}}$ allows for an affine transformation of space in which the governing equation from which the eigenfunctions are obtained is transformed into the Laplace equation. After solving the Laplace equation and obtaining the eigenfunctions in the transformed space, an inverse transformation of space is effected to obtain eigenfunctions in the original space for the material described by Eq. (1). We apply the procedure here to analytically investigate the perturbation of an electrostatic field by the anisotropic dielectric sphere.

The plan of this paper is as follows. Section 2 contains the formulation of the boundary-value problem in terms of the electric potential. The expansion of the potential in the exterior region, which is vacuous, is presented in Sec. 2.1; two illustrative examples of the source potential are provided in Sec. 2.2; the expansion of the potential inside the anisotropic dielectric sphere is derived in Sec. 2.3; boundary conditions are enforced in Secs. 2.4–2.6 to derive a transition matrix that relates the expansion coefficients of the perturbation potential to those of the source potential; the symmetries of the transition matrix are presented in Sec. 2.7; and an asymptotic expression for the perturbation potential is derived in Sec. 2.8. Section 3 presents illustrative numerical results.

2 Boundary-Value Problem

The region $r > a > 0$ is taken to be vacuous with constitutive relation $\mathbf{D}(\mathbf{r}) = \varepsilon_0 \mathbf{E}(\mathbf{r})$, whereas the spherical region $r < a$ is occupied by the chosen material described by Eq. (1). As electrostatic fields always satisfy the relation $\nabla \times \mathbf{E}(\mathbf{r}) = \mathbf{0}$ [2], it follows that $\mathbf{E}(\mathbf{r}) = -\nabla \Phi(\mathbf{r})$, where $\Phi(\mathbf{r})$ is the electric potential. Henceforth, we use the electric potential.

2.1 Potential in the region $r > a$

The solution of the Laplace equation $\nabla^2 \Phi(\mathbf{r}) = 0$ in the spherical coordinate system $\mathbf{r} \equiv (r, \theta, \phi)$ has been known for almost two centuries; thus [2, 16],

$$\Phi(\mathbf{r}) = \sum_{s \in \{e, o\}} \sum_{n=0}^{\infty} \sum_{m=0}^n \left\{ E_{\text{smn}} \left[\mathcal{A}_{\text{smn}} r^n + \mathcal{B}_{\text{smn}} r^{-(n+1)} \right] Y_{\text{smn}}(\theta, \phi) \right\}, \quad r > a, \quad (4)$$

where

$$E_{mn} = (2 - \delta_{m0}) \frac{2n+1}{4\pi} \frac{(n-m)!}{(n+m)!} \quad (5)$$

is a normalization factor with $\delta_{mm'}$ as the Kronecker delta and the tesseral harmonics

$$\left. \begin{aligned} Y_{\text{emn}}(\theta, \phi) &= P_n^m(\cos \theta) \cos(m\phi) \\ Y_{\text{omn}}(\theta, \phi) &= P_n^m(\cos \theta) \sin(m\phi) \end{aligned} \right\} \quad (6)$$

involve the associated Legendre function $P_n^m(\cos \theta)$ [22, 23]. The coefficients \mathcal{A}_{smn} are associated with terms that are regular at the origin, whereas the coefficients \mathcal{B}_{smn} are associated with terms that are regular at infinity. The definitions of the tesseral harmonics mandate that $\mathcal{A}_{00n} = 0$ and $\mathcal{B}_{00n} = 0 \forall n$.

On the right side of Eq. (4),

$$\Phi_{\text{source}}(\mathbf{r}) = \sum_{s \in \{e, o\}} \sum_{n=0}^{\infty} \sum_{m=0}^n [E_{mn} \mathcal{A}_{\text{smn}} r^n Y_{\text{smn}}(\theta, \phi)] \quad (7)$$

is the source potential whereas

$$\Phi_{\text{pert}}(\mathbf{r}) = \sum_{s \in \{e, o\}} \sum_{n=0}^{\infty} \sum_{m=0}^n [E_{mn} \mathcal{B}_{\text{smn}} r^{-(n+1)} Y_{\text{smn}}(\theta, \phi)], \quad r > a, \quad (8)$$

is the perturbation potential. If the object were to be absent, Eq. (4) would hold for all \mathbf{r} with $\mathcal{B}_{\text{smn}} \equiv 0 \forall \{s, m, n\}$.

2.2 Source potential

We proceed with the assumption that the coefficients \mathcal{A}_{smn} are known but the coefficients \mathcal{B}_{smn} are not. Furthermore, Eq. (7) is required to hold in some sufficiently large open region that contains the spherical region $r \leq a$ but not the region containing the source of $\Phi_{\text{source}}(\mathbf{r})$.

Two illustrative examples of sources are a point charge Q and a point dipole \mathbf{p} . Suppose, first, that the source potential is due to a point charge Q located at $\mathbf{r}_o \equiv (r_o, \theta_o, \phi_o)$ with $r_o > a$; then

$$\Phi_{\text{source}}(\mathbf{r}) = \frac{1}{4\pi\epsilon_0} \frac{Q}{|\mathbf{r} - \mathbf{r}_o|}. \quad (9)$$

This potential can be expanded as [2]

$$\Phi_{\text{source}}(\mathbf{r}) = \begin{cases} \sum_{s \in \{e, o\}} \sum_{n=0}^{\infty} \sum_{m=0}^n [E_{mn} \bar{\mathcal{A}}_{\text{smn}} r^{-(n+1)} Y_{\text{smn}}(\theta, \phi)], & r > r_o, \\ \sum_{s \in \{e, o\}} \sum_{n=0}^{\infty} \sum_{m=0}^n [E_{mn} \mathcal{A}_{\text{smn}} r^n Y_{\text{smn}}(\theta, \phi)], & r < r_o, \end{cases} \quad (10)$$

where the coefficients

$$\bar{\mathcal{A}}_{\text{smn}} = \frac{Q}{\epsilon_0} \frac{1}{2n+1} r_o^n Y_{\text{smn}}(\theta_o, \phi_o) \quad (11a)$$

and

$$\mathcal{A}_{\text{smn}} = \frac{Q}{\varepsilon_0} \frac{1}{2n+1} r_o^{-(n+1)} Y_{\text{smn}}(\theta_o, \phi_o). \quad (11b)$$

Suppose, next, that the source potential is due to a point dipole of moment $\mathbf{p} = p\hat{\mathbf{p}}$ located at $\mathbf{r}_o \equiv (r_o, \theta_o, \phi_o)$ with $r_o > a$; then [24]

$$\Phi_{\text{source}}(\mathbf{r}) = \frac{1}{4\pi\varepsilon_0} \mathbf{p} \cdot \nabla_o \left(\frac{1}{|\mathbf{r} - \mathbf{r}_o|} \right), \quad (12)$$

where $\nabla_o(\dots)$ denotes the gradient with respect to \mathbf{r}_o . Equation (10) still holds, but with

$$\bar{\mathcal{A}}_{\text{smn}} = \frac{p}{\varepsilon_0} \frac{1}{2n+1} \hat{\mathbf{p}} \cdot \nabla_o [r_o^n Y_{\text{smn}}(\theta_o, \phi_o)] \quad (13a)$$

and

$$\mathcal{A}_{\text{smn}} = \frac{p}{\varepsilon_0} \frac{1}{2n+1} \hat{\mathbf{p}} \cdot \nabla_o [r_o^{-(n+1)} Y_{\text{smn}}(\theta_o, \phi_o)]. \quad (13b)$$

2.3 Potential in the region $r < a$

Inside the dielectric sphere, the potential $\Phi(\mathbf{r})$ does not obey the Laplace equation; instead,

$$\nabla \cdot [\underline{\underline{A}} \cdot \underline{\underline{A}} \cdot \nabla \Phi(\mathbf{r})] = 0. \quad (14)$$

In order to solve this equation, let us make an affine coordinate transformation:

$$\underline{\underline{A}}^{-1} \cdot \mathbf{r} = \mathbf{r}_q \equiv (r_q, \theta_q, \phi_q), \quad (15)$$

where

$$r_q = |\underline{\underline{A}}^{-1} \cdot \mathbf{r}| = r \sqrt{(\alpha_x^2 \cos^2 \phi + \alpha_y^2 \sin^2 \phi) \sin^2 \theta + \cos^2 \theta} \geq 0, \quad (16a)$$

$$\theta_q = \cos^{-1} \left(\frac{r}{|\underline{\underline{A}}^{-1} \cdot \mathbf{r}|} \cos \theta \right), \quad (16b)$$

and

$$\phi_q = \tan^{-1} \left(\frac{\alpha_y}{\alpha_x} \tan \phi \right). \quad (16c)$$

The bijective transformation (15) maps a sphere into an ellipsoid since $\alpha_x > 0$ and $\alpha_y > 0$, with θ_q lying in the same quadrant as θ and ϕ_q in the same quadrant as ϕ .

Then, Eq. (14) can be written as

$$\nabla_q \cdot [\nabla_q \Phi(\mathbf{r}_q)] = 0, \quad (17)$$

i.e.,

$$\nabla_q^2 \Phi(\mathbf{r}_q) = 0, \quad (18)$$

which is the Laplace equation in the transformed space. Its solution is given by [2, 16]

$$\Phi(\mathbf{r}_q) = \sum_{s \in \{e, o\}} \sum_{n=0}^{\infty} \sum_{m=0}^n \left\{ E_{\text{mn}} \left[\mathcal{C}_{\text{smn}} r_q^n + \mathcal{D}_{\text{smn}} r_q^{-(n+1)} \right] Y_{\text{smn}}(\theta_q, \phi_q) \right\}. \quad (19)$$

We must set $\mathcal{D}_{\text{snn}} \equiv 0$ in order to exclude terms on the right side of Eq. (19) that are not regular at the origin. Thereafter, on inverting the coordinate transformation, we obtain the internal potential

$$\Phi_{\text{int}}(\mathbf{r}) = \sum_{s \in \{e, o\}} \sum_{n=0}^{\infty} \sum_{m=0}^n [E_{\text{mn}} \mathcal{C}_{\text{snn}} Z_{\text{snn}}(\mathbf{r})], \quad r < a, \quad (20)$$

where

$$\left. \begin{aligned} Z_{\text{emn}}(\mathbf{r}) &= |\underline{\underline{A}}^{-1} \cdot \mathbf{r}|^n P_n^m \left[\frac{r}{|\underline{\underline{A}}^{-1} \cdot \mathbf{r}|} \cos \theta \right] \cos \left[m \tan^{-1} \left(\frac{\alpha_y}{\alpha_x} \tan \phi \right) \right] \\ Z_{\text{omn}}(\mathbf{r}) &= |\underline{\underline{A}}^{-1} \cdot \mathbf{r}|^n P_n^m \left[\frac{r}{|\underline{\underline{A}}^{-1} \cdot \mathbf{r}|} \cos \theta \right] \sin \left[m \tan^{-1} \left(\frac{\alpha_y}{\alpha_x} \tan \phi \right) \right] \end{aligned} \right\}. \quad (21)$$

2.4 Boundary conditions

Since the tangential component of the electric field must be continuous across the interface $r = a$, and as there is no reason for the electric field to have an infinite magnitude anywhere on that interface, the potential must be continuous across that interface; hence,

$$\Phi_{\text{source}}(r, \theta, \phi) + \Phi_{\text{pert}}(r, \theta, \phi) = \Phi_{\text{int}}(r, \theta, \phi), \quad r = a, \quad \theta \in [0, \pi], \quad \phi \in [0, 2\pi). \quad (22)$$

Likewise, with the assumption of the interface $r = a$ being charge-free, the normal component of the electric displacement must be continuous across that interface; hence,

$$\frac{\partial}{\partial r} [\Phi_{\text{source}}(r, \theta, \phi) + \Phi_{\text{pert}}(r, \theta, \phi)] = \varepsilon_r \hat{\mathbf{r}} \cdot \underline{\underline{A}} \cdot \underline{\underline{A}} \cdot \nabla \Phi_{\text{int}}(r, \theta, \phi), \quad r = a, \quad \theta \in [0, \pi], \quad \phi \in [0, 2\pi), \quad (23)$$

where $\hat{\mathbf{r}} = (\hat{\mathbf{x}} \cos \phi + \hat{\mathbf{y}} \sin \phi) \sin \theta + \hat{\mathbf{z}} \cos \theta$.

2.5 Transition matrix

After (i) substituting Eqs. (7), (8), and (20) in Eq. (22), (ii) then multiplying both sides of the resulting equation by $Y_{s'm'n'}(\theta, \phi) \sin \theta$, and (iii) finally integrating over $\theta \in [0, \pi]$ and $\phi \in [0, 2\pi)$, we get

$$\sum_{\text{snn}} [\mathcal{A}_{\text{snn}} \mathcal{I}_{\text{ss'mm'nn'}} + \mathcal{B}_{\text{snn}} \mathcal{J}_{\text{ss'mm'nn'}}] = \sum_{\text{snn}} [\mathcal{C}_{\text{snn}} \mathcal{K}_{\text{ss'mm'nn'}}], \quad (24)$$

where

$$\mathcal{I}_{\text{ss'mm'nn'}} = a^n \delta_{ss'} \delta_{mm'} \delta_{nn'}, \quad (25a)$$

$$\mathcal{J}_{\text{ss'mm'nn'}} = a^{-(n+1)} \delta_{ss'} \delta_{mm'} \delta_{nn'}, \quad (25b)$$

and

$$\mathcal{K}_{\text{ss'mm'nn'}} = E_{\text{mn}} \int_{\phi=0}^{2\pi} \int_{\theta=0}^{\pi} Z_{\text{snn}}(a, \theta, \phi) Y_{s'm'n'}(\theta, \phi) \sin \theta \, d\theta \, d\phi. \quad (25c)$$

Similarly, after (i) substituting Eqs. (7), (8), and (20) in Eq. (23), (ii) then multiplying both sides of the resulting equation by $Y_{s'm'n'}(\theta, \phi) \sin \theta$, and (iii) finally integrating over $\theta \in [0, \pi]$ and $\phi \in [0, 2\pi)$, we get

$$\sum_{\text{snn}} [\mathcal{A}_{\text{snn}} \mathcal{L}_{\text{ss'mm'nn'}} + \mathcal{B}_{\text{snn}} \mathcal{M}_{\text{ss'mm'nn'}}] = \sum_{\text{snn}} [\mathcal{C}_{\text{snn}} \mathcal{N}_{\text{ss'mm'nn'}}], \quad (26)$$

where

$$\mathcal{L}_{ss'mm'nn'} = na^{n-1} \delta_{ss'} \delta_{mm'} \delta_{nn'}, \quad (27a)$$

$$\mathcal{M}_{ss'mm'nn'} = -(n+1)a^{-(n+2)} \delta_{ss'} \delta_{mm'} \delta_{nn'}, \quad (27b)$$

and

$$\mathcal{N}_{ss'mm'nn'} = \varepsilon_r E_{\text{mn}} \int_{\phi=0}^{2\pi} \int_{\theta=0}^{\pi} \hat{\mathbf{r}} \cdot \underline{\underline{\mathbf{A}}} \cdot \underline{\underline{\mathbf{A}}} \cdot \left\{ [\nabla Z_{\text{smn}}(\mathbf{r})] \Big|_{r=a} \right\} Y_{s'm'n'}(\theta, \phi) \sin \theta \, d\theta \, d\phi, \quad (27c)$$

After truncating the indexes n and n' so that only $n \in [0, N]$ and $n' \in [0, N]$ are considered with $N > 0$, Eqs. (24) and (26) can be put together in matrix form symbolically as

$$\begin{bmatrix} \mathcal{I} & \mathcal{J} \\ \mathcal{L} & \mathcal{M} \end{bmatrix} \begin{bmatrix} \mathcal{A} \\ \mathcal{B} \end{bmatrix} = \begin{bmatrix} \mathcal{K} \\ \mathcal{N} \end{bmatrix} [\mathcal{C}], \quad (28)$$

which leads to the solution

$$\begin{bmatrix} \mathcal{C} \\ \mathcal{B} \end{bmatrix} = \begin{bmatrix} \mathcal{K} & -\mathcal{J} \\ \mathcal{N} & -\mathcal{M} \end{bmatrix}^{-1} \begin{bmatrix} \mathcal{I} \\ \mathcal{L} \end{bmatrix} [\mathcal{A}]. \quad (29)$$

Thus, the coefficients \mathcal{B}_{smn} and \mathcal{C}_{smn} can be determined in terms of the coefficients \mathcal{A}_{smn} .

The perturbational characteristics of the anisotropic dielectric sphere are encapsulated in the transition matrix \mathcal{T} that relates the column vectors \mathcal{B} and \mathcal{A} via

$$\mathcal{B} = \mathcal{T} \mathcal{A}, \quad (30)$$

where

$$\mathcal{T} = -\mathcal{J}^{-1} (\mathcal{M} \mathcal{J}^{-1} - \mathcal{N} \mathcal{K}^{-1})^{-1} (\mathcal{L} \mathcal{I}^{-1} - \mathcal{N} \mathcal{K}^{-1}) \mathcal{I}. \quad (31)$$

The transition matrix is a diagonal matrix when the sphere is made of an isotropic dielectric material (i.e., $\underline{\underline{\mathbf{A}}} = \underline{\underline{\mathbf{I}}}$) because $\mathcal{N} \mathcal{K}^{-1}$ is then a diagonal matrix. In general, $\mathcal{N} \mathcal{K}^{-1}$ is not a diagonal matrix when the sphere is made of an anisotropic dielectric material, so that \mathcal{T} is not a diagonal matrix either.

2.6 Reduction of computational effort

Computational effort for the integrals (25c) and (27c) can be significantly reduced on noting that

$$\left. \begin{aligned} \sin[m(\pi + \phi)] &= (-)^m \sin(m\phi), & \sin[m(\pi + \phi_q)] &= (-)^m \sin(m\phi_q) \\ \cos[m(\pi + \phi)] &= (-)^m \cos(m\phi), & \cos[m(\pi + \phi_q)] &= (-)^m \cos(m\phi_q) \\ P_n^m[\cos(\pi - \theta)] &= (-)^{n+m} P_n^m(\cos \theta), & P_n^m[\cos(\pi - \theta_q)] &= (-)^{n+m} P_n^m(\cos \theta_q) \end{aligned} \right\}; \quad (32)$$

furthermore, θ_q lies in the same quadrant as θ and ϕ_q in the same quadrant as ϕ . Therefore,

$$\begin{aligned} \mathcal{K}_{ss'mm'nn'} &= \left[1 + (-)^{m+m'} \right] \left[1 + (-)^{m+m'+n+n'} \right] E_{\text{mn}} \\ &\quad \times \int_{\phi=0}^{\pi} \int_{\theta=0}^{\pi/2} Z_{\text{smn}}(a, \theta, \phi) Y_{s'm'n'}(\theta, \phi) \sin \theta \, d\theta \, d\phi \end{aligned} \quad (33)$$

and

$$\begin{aligned} \mathcal{N}_{ss'mm'nn'} &= \left[1 + (-)^{m+m'}\right] \left[1 + (-)^{m+m'+n+n'}\right] \varepsilon_r E_{mn} \\ &\times \int_{\phi=0}^{\pi} \int_{\theta=0}^{\pi/2} \hat{\mathbf{r}} \cdot \underline{\underline{\mathbf{A}}} \cdot \underline{\underline{\mathbf{A}}} \cdot \left\{ [\nabla Z_{smn}(\mathbf{r})] \Big|_{r=a} \right\} Y_{s'm'n'}(\theta, \phi) \sin \theta \, d\theta \, d\phi \end{aligned} \quad (34)$$

can be used instead of Eqs. (25c) and (27c), respectively.

2.7 Symmetries of the transition matrix

By virtue of its definition through Eq. (30), the transition matrix \mathcal{T} does not depend on the source potential. This matrix depends only on the radius a and the constitutive parameters α_x , α_y , and ε_r of the perturbing sphere.

Let us denote each element of the transition matrix defined in Eq. (31) by $\mathcal{T}_{ss'mm'nn'}$. It was verified numerically that $\mathcal{T}_{ss'mm'nn'} \neq 0$ if the following three conditions are satisfied:

- (i) $s = s'$,
- (ii) m and m' have the same parity (i.e., even or odd), and
- (iii) n and n' have the same parity.

Finally, let the transition matrix elements be denoted as $\mathcal{T}_{ss'mm'nn'}^{(a)}$ for a specific choice $\{\alpha_x, \alpha_y\}$ of the anisotropy parameters, but as $\mathcal{T}_{ss'mm'nn'}^{(b)}$ after α_x and α_y have been interchanged without changing ε_r . In other words, $\mathcal{T}_{ss'mm'nn'}^{(a)}$ changes to $\mathcal{T}_{ss'mm'nn'}^{(b)}$ when the sphere is rotated about the z axis by $\pi/2$. Then, the following relationships exist between the pre- and post-rotation transition matrixes:

- $\mathcal{T}_{ssmmnn'}^{(a)} = \mathcal{T}_{ssmmnn'}^{(b)}$ when m is even,
- $\mathcal{T}_{eemmmn'}^{(a)} = \mathcal{T}_{oommmn'}^{(b)}$ and $\mathcal{T}_{oommmn'}^{(a)} = \mathcal{T}_{eemmmn'}^{(b)}$ when m is odd,
- $\mathcal{T}_{ssmm'nn'}^{(a)} = -\mathcal{T}_{ssmm'nn'}^{(b)}$ when $m \neq m'$ and both are even, and
- $\mathcal{T}_{eemmm'nn'}^{(a)} = -\mathcal{T}_{oommm'nn'}^{(b)}$ and $\mathcal{T}_{oommm'nn'}^{(a)} = -\mathcal{T}_{eemmm'nn'}^{(b)}$ when $m \neq m'$ and both are odd.

2.8 Asymptotic expression for perturbation potential

Equation (8) can be written as

$$\begin{aligned} \Phi_{\text{pert}}(\mathbf{r}) &= \frac{1}{4\pi} \left\{ r^{-1} \mathcal{B}_{e00} + 3r^{-2} [\mathcal{B}_{e01} \cos \theta + 2(\mathcal{B}_{e11} \cos \phi + \mathcal{B}_{o11} \sin \phi) \sin \theta] \right\} \\ &+ \sum_{s \in \{e,o\}} \sum_{n=2}^{\infty} \sum_{m=0}^n \left[E_{mn} \mathcal{B}_{smn} r^{-(n+1)} Y_{smn}(\theta, \phi) \right], \quad r > a. \end{aligned} \quad (35)$$

Since $\mathcal{B}_{e00} = 0$ emerges from calculations for a sphere whether $\underline{\underline{A}} = \underline{\underline{I}}$ or not, the asymptotic behavior of the perturbation potential far away from the sphere is given by

$$\Phi_{\text{pert}}(r, \theta, \phi) = \frac{f_{\text{pert}}(\theta, \phi)}{r^2} + \mathcal{O}\left(\frac{1}{r^3}\right), \quad r \rightarrow \infty, \quad (36)$$

where the asymptotic perturbation

$$f_{\text{pert}}(\theta, \phi) = \frac{3}{4\pi} [\mathcal{B}_{e01} \cos \theta + 2(\mathcal{B}_{e11} \cos \phi + \mathcal{B}_{o11} \sin \phi) \sin \theta]. \quad (37)$$

Accordingly, the first term on the right side of Eq. (37) does not exist in the equatorial plane (i.e., $\theta = \pi/2$) whereas the second term is absent on the z axis (i.e., $\theta \in \{0, \pi\}$).

Now, the perturbation potential $\Phi_{\text{pert}}(r, \theta, \phi)$ must depend on the source as well as on the radius a of the sphere. For the two sources chosen for illustrative results, f_{pert} must depend linearly on both the sign and the magnitude of Q or p (as appropriate). The location of either of the two sources enters the potential expressions only by means of the source-potential coefficients \mathcal{A}_{smn} , which are proportional to $r_o^{-(n+1)}$ for the point charge and to $r_o^{-(n+2)}$ for the point dipole, according to Eqs. (11b) and (13b). Since the transition matrix \mathcal{T} does not depend on the source, the perturbation-potential coefficients \mathcal{B}_{e01} , \mathcal{B}_{e11} , and \mathcal{B}_{o11} increase/decrease as r_o decreases/increases. Accordingly, the magnitude of f_{pert} increases/decreases as r_o decreases/increases.

Furthermore, from Eqs. (25a), (25b), (27a), and (27b), we get

$$\left. \begin{aligned} \mathcal{I}_{ss'mm'nn'} &\propto a^n, & \mathcal{J}_{ss'mm'nn'} &\propto a^{-(n+1)} \\ \mathcal{L}_{ss'mm'nn'} &\propto a^{n-1}, & \mathcal{M}_{ss'mm'nn'} &\propto a^{-(n+2)} \end{aligned} \right\}. \quad (38)$$

Since the coefficients \mathcal{A}_{smn} cannot depend on a , it follows then from Eqs. (24) and (26) that

$$\mathcal{B}_{\text{smn}} \propto a^{2n+1}. \quad (39)$$

Dimensional analysis of Eq. (4) also supports this proportionality. Equations (37) and (39) then yield accordingly,

$$f_{\text{pert}}(\theta, \phi) \propto a^3. \quad (40)$$

3 Numerical Results and Discussion

3.1 Preliminaries

For all numerical results presented in this section, we fixed

$$\varepsilon_r = \frac{3\varepsilon_{\text{ave}}}{\alpha_x^{-2} + \alpha_y^{-2} + 1}, \quad (41)$$

and $\varepsilon_{\text{ave}} = 3$. Note that $\varepsilon_r = \varepsilon_{\text{ave}}$ when the sphere is made of an isotropic material (i.e., $\underline{\underline{A}} = \underline{\underline{I}}$).

A Mathematica™ program was written to calculate the normalized functions

$$\tilde{\Phi}_{\text{pert}}(r, \theta, \phi) = \tilde{r}^2 \Phi_{\text{pert}}(r, \theta, \phi) \quad (42a)$$

and

$$F_{\text{pert}}(\theta, \phi) = \frac{f_{\text{pert}}(\theta, \phi)}{\pi a^2 \Phi_{\text{source}}^{\text{ref}}}, \quad (42b)$$

where the normalized radius $\tilde{r} = r/a$ and $\Phi_{\text{source}}^{\text{ref}} \neq 0$ is some reference value of the source potential. The reference value can be chosen as $\Phi_{\text{source}}^{\text{ref}} = \Phi_{\text{source}}(\mathbf{0}) = \mathcal{A}_{e00}/4\pi$. This choice works well if the source is an external point charge and also if the source is an external point dipole except when $\mathbf{p} \cdot \mathbf{r}_o = 0$. By virtue of its definition and the dependencies of f_{pert} discussed in Sec. 2.8, F_{pert}

- (i) is independent of Q or p (as appropriate),
- (ii) increases/decreases as r_o decreases/increases, and
- (iii) is directly proportional to a .

A convergence test was carried out with respect to N , by calculating the integral

$$I(\tilde{r}) = \int_{\phi=0}^{2\pi} \int_{\theta=0}^{\pi} \tilde{\Phi}_{\text{pert}}^2(\tilde{r} a, \theta, \phi) \sin \theta \, d\theta \, d\phi, \quad (43)$$

at diverse values of $\tilde{r} > 1$ as N was incremented by unity. The iterative process of increasing N was terminated when $I(\tilde{r})$ within a preset tolerance of 1%. The adequate value of N was higher for lower \tilde{r} , with $N = 5$ sufficient for $\tilde{r} \geq 5$.

The theory described in Sec. 2 was validated by comparing its results for the perturbation of the source potential by an isotropic dielectric sphere with the corresponding exact solutions available in the literature. First, the source was taken to be a point charge located on the $+z$ axis (i.e. $\theta_o = 0$) at $r_o = 10a$; note that ϕ_o is irrelevant when $\sin \theta_o = 0$. Excellent agreement was obtained with respect to the exact solution [25] for all examined values of a and ε_r . Next, the point charge was replaced by a point dipole. Again, excellent agreement was found with respect to the corresponding exact solutions [24, 26].

3.2 Normalized asymptotic perturbation $F_{\text{pert}}(\theta, \phi)$

Having clarified in Sec. 3.1 the effects of the parameters Q , p , r_o , and a on the normalized asymptotic perturbation $F_{\text{pert}}(\theta, \phi)$, we present next numerical results for the variations of $F_{\text{pert}}(\theta, \phi)$ as a function of the sphere's anisotropy parameters α_x and α_y for the following three cases:

Case 1: $\alpha_x \neq \alpha_y = 1$,

Case 2: $\alpha_y \neq \alpha_x = 1$, and

Case 3: $\alpha_x = \alpha_y \neq 1$.

Plots of the perturbation-potential coefficients \mathcal{B}_{e01} , \mathcal{B}_{e11} , and \mathcal{B}_{o11} as functions of α_x and α_y are examined in conjunction with the corresponding plots of $F_{\text{pert}}(\theta, \phi)$ versus θ and ϕ for $a = 5$ cm, $r_o = 2a$, $\theta_o = \pi/4$, and $\phi_o = \pi/3$. All calculations were made for either a point charge of magnitude $Q = 10^{-10}$ C or a point dipole of moment $p = 10^{-10}$ C m.

3.2.1 Case 1 ($\alpha_x = \bar{\alpha}$, $\alpha_y = 1$)

We varied $\alpha_x = \bar{\alpha} \in [0.5, 1.5]$ but kept $\alpha_y = 1$ fixed. Figure 1 shows plots of \mathcal{B}_{e01} , \mathcal{B}_{e11} , and \mathcal{B}_{o11} versus $\bar{\alpha}$ for a point-charge source as well as for a point-dipole source with $\hat{\mathbf{p}} \in \{\hat{\mathbf{x}}, \hat{\mathbf{y}}, \hat{\mathbf{z}}\}$. Angular profiles of the $F_{\text{pert}}(\theta, \phi)$ for the same sources are depicted in Fig. 2 for $\bar{\alpha} = 0.5$, and in Fig. 3 for $\bar{\alpha} = 1.5$.

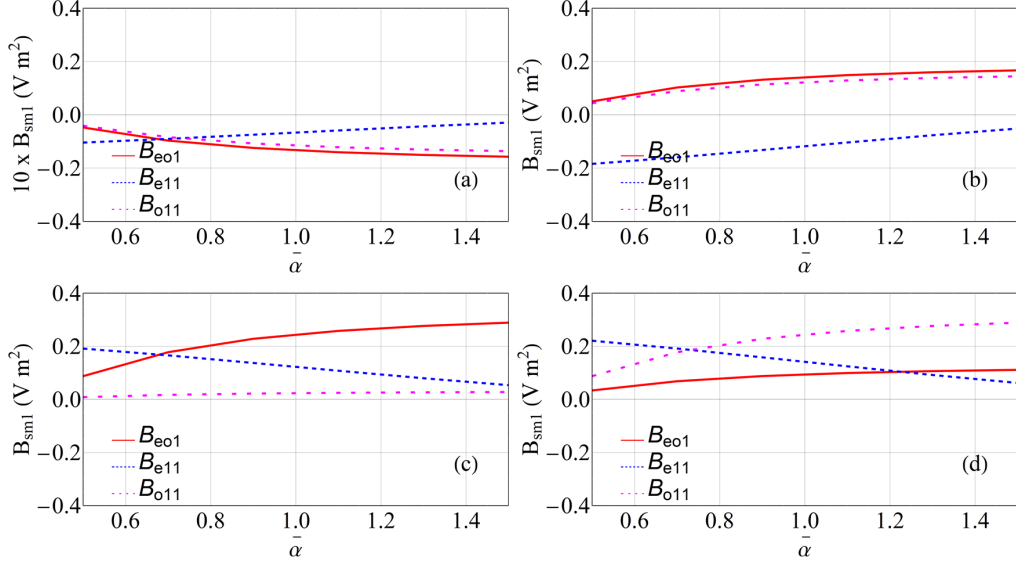


Figure 1: \mathcal{B}_{e01} , \mathcal{B}_{e11} , and \mathcal{B}_{o11} vs $\bar{\alpha} \in [0.5, 1.5]$ when $\alpha_x = \bar{\alpha}$, $\alpha_y = 1$, and the source is either (a) a point charge or (b-d) a point dipole with (b) $\hat{\mathbf{p}} = \hat{\mathbf{x}}$, (c) $\hat{\mathbf{p}} = \hat{\mathbf{y}}$, and (d) $\hat{\mathbf{p}} = \hat{\mathbf{z}}$, respectively.

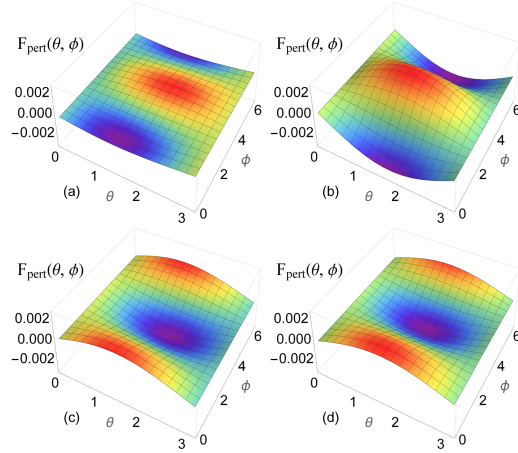


Figure 2: $F_{\text{pert}}(\theta, \phi)$ vs θ and ϕ when $\alpha_x = 0.5$, $\alpha_y = 1$, and the source is either (a) a point charge or (b-d) a point dipole with (b) $\hat{\mathbf{p}} = \hat{\mathbf{x}}$, (c) $\hat{\mathbf{p}} = \hat{\mathbf{y}}$, and (d) $\hat{\mathbf{p}} = \hat{\mathbf{z}}$, respectively.

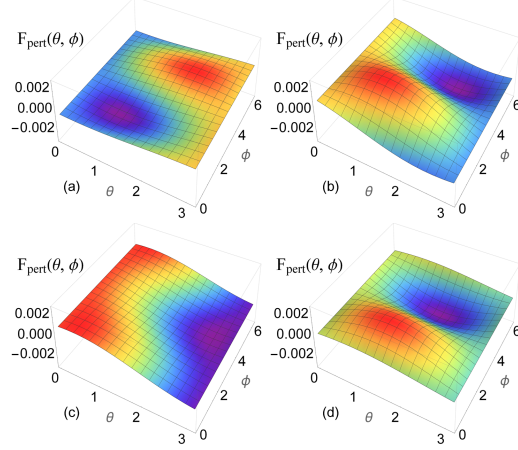


Figure 3: As in Fig. 2, except for $\alpha_x = 1.5$.

For a point-charge source, \mathcal{B}_{e01} decreases with $\bar{\alpha} \in [0.5, 1.5]$ in Fig. 1(a). Thus, $F_{\text{pert}}(0, \phi)$ decreases but $F_{\text{pert}}(\pi, \phi)$ increases as α_x changes from 0.5 to 1.5, as can be gathered from Figs. 2(a) and 3(a). Also, \mathcal{B}_{e11} increases and \mathcal{B}_{o11} decreases with increasing α_x . Therefore, $F_{\text{pert}}(\pi/2, 0)$ increases but $F_{\text{pert}}(\pi/2, \pi/2)$ decreases as α_x changes from 0.5 to 1.5.

Next, for the point-dipole sources, \mathcal{B}_{e01} increases with increasing $\bar{\alpha} \in [0.5, 1.5]$ for all three dipole orientations, as is clear from Figs. 1(b)–(d); the largest increase is observed for $\hat{\mathbf{p}} = \hat{\mathbf{y}}$. Hence, a comparison of Figs. 2(b)–(d) and 3(b)–(d) reveals that $F_{\text{pert}}(0, \phi)$ increases but $F_{\text{pert}}(\pi, \phi)$ decreases as α_x changes from 0.5 to 1.5. The rate of these increases or decreases is highest for $\hat{\mathbf{p}} = \hat{\mathbf{y}}$, moderate for $\hat{\mathbf{p}} = \hat{\mathbf{x}}$, and lowest for $\hat{\mathbf{p}} = \hat{\mathbf{z}}$.

Besides, for $\hat{\mathbf{p}} = \hat{\mathbf{x}}$, both \mathcal{B}_{e11} and \mathcal{B}_{o11} increase with α_x in Fig. 1(b) and, thus, $F_{\text{pert}}(\pi/2, 0)$ and $F_{\text{pert}}(\pi/2, \pi/2)$ also increase with α_x in Figs. 2(b) and 3(b). On the other hand, for $\hat{\mathbf{p}} = \hat{\mathbf{y}}$ and $\hat{\mathbf{p}} = \hat{\mathbf{z}}$, \mathcal{B}_{e11} decreases in Figs. 1(c) but \mathcal{B}_{o11} increases in Fig. 1(d) as α_x increases. Therefore, $F_{\text{pert}}(\pi/2, 0)$ decreases and $F_{\text{pert}}(\pi/2, \pi/2)$ increases with α_x , as can be gathered from comparing Figs. 2(c) and (d) with Figs. 3(c) and (d), respectively.

3.2.2 Case 2 ($\alpha_x = 1$, $\alpha_y = \bar{\alpha}$)

Next, we fixed $\alpha_x = 1$ but varied $\alpha_y \in [0.5, 1.5]$. The dependencies of the coefficients \mathcal{B}_{e01} , \mathcal{B}_{e11} , and \mathcal{B}_{o11} on α_y are depicted in Fig. 4, whereas the angular profiles of $F_{\text{pert}}(\theta, \phi)$ are depicted in Fig. 5 for $\alpha_y = 0.5$ and Fig. 6 for $\alpha_y = 1.5$.

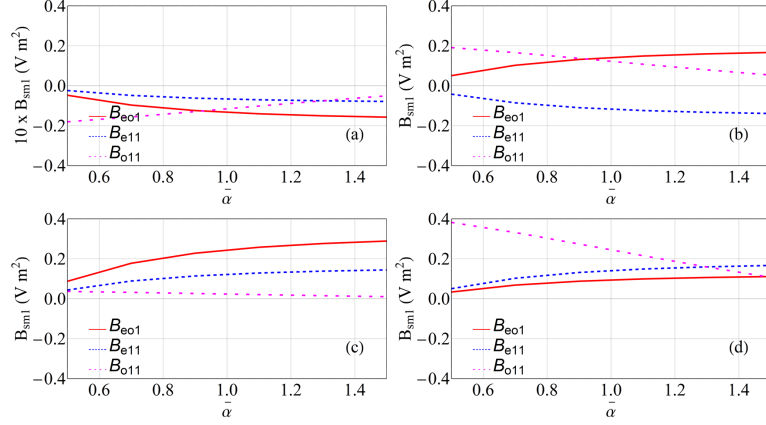


Figure 4: \mathcal{B}_{e01} , \mathcal{B}_{e11} , and \mathcal{B}_{o11} vs $\bar{\alpha} \in [0.5, 1.5]$ when $\alpha_x = 1$, $\alpha_y = \bar{\alpha}$, and the source is either (a) a point charge or (b-d) a point dipole with (b) $\hat{\mathbf{p}} = \hat{\mathbf{x}}$, (c) $\hat{\mathbf{p}} = \hat{\mathbf{y}}$, and (d) $\hat{\mathbf{p}} = \hat{\mathbf{z}}$, respectively.

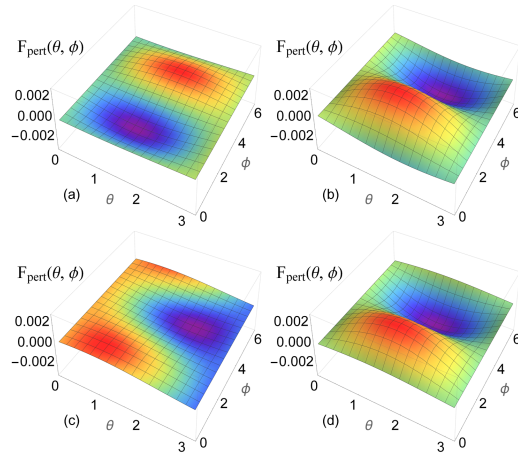


Figure 5: As in Fig. 2, except for $\alpha_x = 1$ and $\alpha_y = 0.5$.

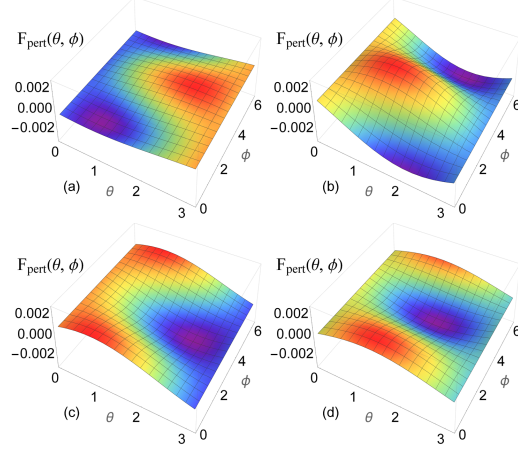


Figure 6: As in Fig. 5, except for $\alpha_y = 1.5$.

For all four types of source considered, \mathcal{B}_{e01} varies with $\bar{\alpha}$ in Case 1 in the same way as it varies with $\bar{\alpha}$ in Case 2. Hence, the characteristics of $F_{\text{pert}}(0, \phi)$ and $F_{\text{pert}}(\pi, \phi)$ in Case 2 replicate those in Case 1. Also, if \mathcal{B}_{e11} or \mathcal{B}_{o11} is an increasing (decreasing) function of $\bar{\alpha}$ in Case 1, then it is a decreasing (increasing) function of $\bar{\alpha}$ in Case 2. Therefore, the characteristics of $F_{\text{pert}}(\pi/2, 0)$ and $F_{\text{pert}}(\pi/2, \pi/2)$ in Case 2 are opposed to those in Case 1.

3.2.3 Case 3 ($\alpha_x = \alpha_y = \bar{\alpha}$)

Finally, we set $\alpha_x = \alpha_y = \bar{\alpha}$. The corresponding plots for \mathcal{B}_{smn} vs $\bar{\alpha} \in [0.5, 1.5]$ are depicted in Figure 7, and for $F_{\text{pert}}(\theta, \phi)$ vs θ and ϕ are depicted in Fig. 8 for $\bar{\alpha} = 0.5$, and in Fig. 9 for $\bar{\alpha} = 1.5$.

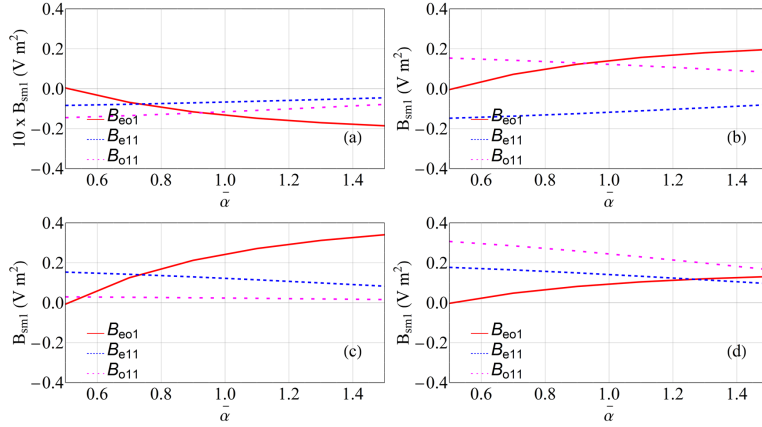


Figure 7: As in Fig. 1, except for $\alpha_x = \alpha_y = \bar{\alpha}$.

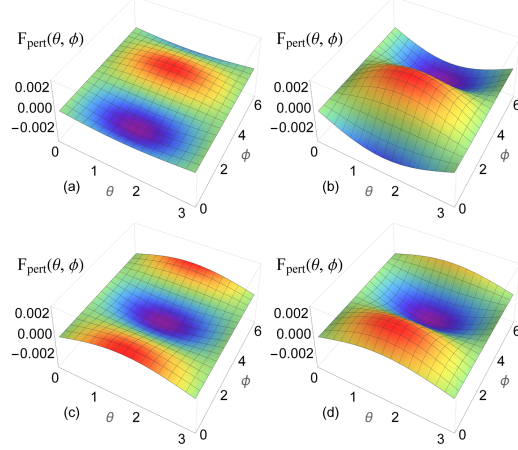


Figure 8: As in Fig. 2, except for $\alpha_x = \alpha_y = 0.5$.

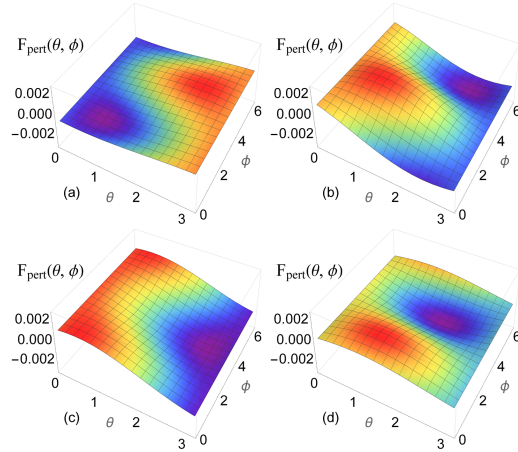


Figure 9: As in Fig. 8, except for $\alpha_x = \alpha_y = 1.5$.

The curves of \mathcal{B}_{e01} vs $\bar{\alpha} \in [0.5, 1.5]$ have the same increasing/decreasing tendencies with the respective ones in Cases 1 and 2; however, the values of \mathcal{B}_{e01} and the rate of increase/decrease w.r.t. $\bar{\alpha}$ are definitely different. Furthermore, in Case 3, the increasing/decreasing tendencies of \mathcal{B}_{e11} and \mathcal{B}_{o11} with $\bar{\alpha}$ are as those in Cases 1 and 2, respectively.

3.3 Normalized perturbation potential $\tilde{\Phi}_{\text{pert}}(r, \theta, \phi)$

Unlike $F_{\text{pert}}(\theta, \phi)$, the normalized perturbation potential $\tilde{\Phi}_{\text{pert}}(r, \theta, \phi)$ depends additionally on the distance $r > a$ from the origin to the observation point. With the same values of a , r_o , θ_o , ϕ_o , Q , and p as in Sec. 3.2, we also examined the perturbation potential's variations with respect to $\tilde{r} = r/a$, with $\alpha_x = 1.2$ and $\alpha_y = 1.6$ fixed, for a point-charge source as well as for a point-dipole source with $\hat{\mathbf{p}} \in \{\hat{\mathbf{x}}, \hat{\mathbf{y}}, \hat{\mathbf{z}}\}$. Figure 10 presents the angular profiles of $\Delta\tilde{\Phi}_{\text{pert}}(25a, 5a, \theta, \phi)$, Fig. 11 of $\Delta\tilde{\Phi}_{\text{pert}}(50a, 25a, \theta, \phi)$, and Fig. 12 of $\Delta\tilde{\Phi}_{\text{pert}}(100a, 50a, \theta, \phi)$, where

$$\Delta\tilde{\Phi}_{\text{pert}}(r_b, r_a, \theta, \phi) = |\tilde{\Phi}_{\text{pert}}(r_b, \theta, \phi) - \tilde{\Phi}_{\text{pert}}(r_a, \theta, \phi)|. \quad (44)$$

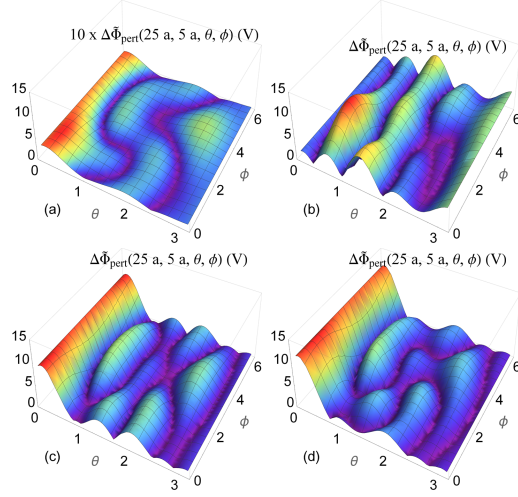


Figure 10: $\Delta\tilde{\Phi}_{\text{pert}}(25a, 5a, \theta, \phi)$ versus θ and ϕ when $\alpha_x = 1.2$, $\alpha_y = 1.6$, and the source is either (a) a point charge or (b-d) a point dipole with (b) $\hat{\mathbf{p}} = \hat{\mathbf{x}}$, with (b) $\hat{\mathbf{p}} = \hat{\mathbf{x}}$, (c) $\hat{\mathbf{p}} = \hat{\mathbf{y}}$, and (d) $\hat{\mathbf{p}} = \hat{\mathbf{z}}$, respectively.

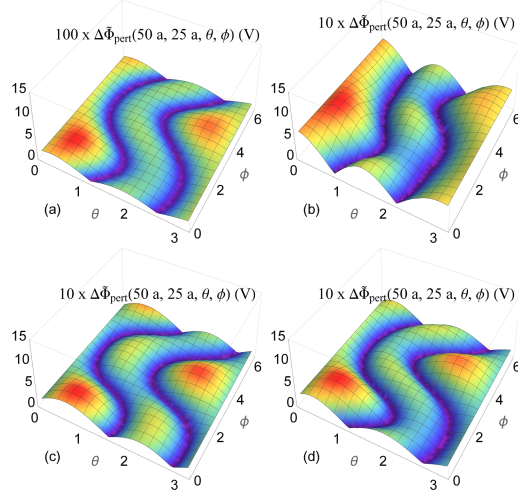


Figure 11: As in Fig. 10, but for $\Delta\tilde{\Phi}_{\text{pert}}(50a, 25a, \theta, \phi)$.

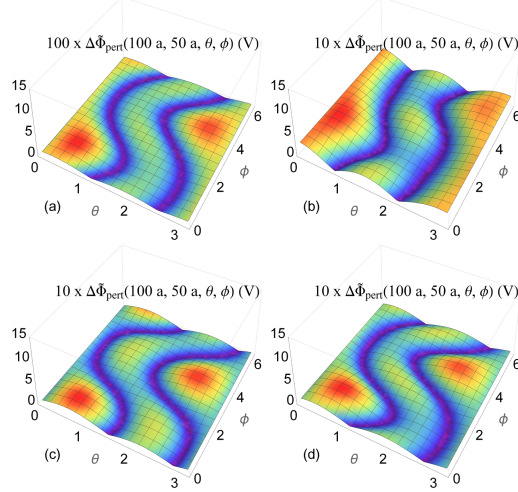


Figure 12: As in Fig. 10, but for $\Delta\tilde{\Phi}_{\text{pert}}(100a, 50a, \theta, \phi)$.

For all four sources, the inequalities $\Delta\tilde{\Phi}_{\text{pert}}(25a, 5a, \theta, \phi) > \Delta\tilde{\Phi}_{\text{pert}}(50a, 25a, \theta, \phi) > \Delta\tilde{\Phi}_{\text{pert}}(100a, 50a, \theta, \phi)$ hold true. This indicates that, as \tilde{r} increases, $\tilde{\Phi}_{\text{pert}}(r, \theta, \phi)$ decreases as expected in every direction (indicated by $\{\theta, \phi\}$). Also, the surface of $\Delta\tilde{\Phi}_{\text{pert}}(100a, 50a, \theta, \phi)$ is smoother and less undulating than the surface of $\Delta\tilde{\Phi}_{\text{pert}}(50a, 25a, \theta, \phi)$, which is smoother and flatter than the surface of $\Delta\tilde{\Phi}_{\text{pert}}(25a, 5a, \theta, \phi)$. This is due to the waning of the higher-order terms on the right side of Eq. (35) as \tilde{r} increases. These higher-order terms have a strong effect on $\Phi_{\text{pert}}(r, \theta, \phi)$ at observation points close to the sphere, the strongest such effects being observed for the dipole sources, as is evident from Figs. 10(b)–(d). Indeed, the decrease of $\tilde{\Phi}_{\text{pert}}(r, \theta, \phi)$ and the smoothing of its angular profile with increase of \tilde{r} is reflected in the limit

$$\lim_{r \rightarrow \infty} \tilde{\Phi}_{\text{pert}}(r, \theta, \phi) = \pi \Phi_{\text{source}}^{\text{ref}} F_{\text{pert}}(\theta, \phi). \quad (45)$$

Finally, on comparing Figs. 10–12, we observe that the portions of the θ - ϕ plane corresponding to the maximum/minimum increase in $|\tilde{\Phi}_{\text{pert}}(r, \theta, \phi)|$ remain almost the same as \tilde{r} increases, for each of the four source potentials considered.

4 Concluding Remarks

We formulated and solved the boundary-value problem for the perturbation of an electric potential by a homogeneous anisotropic dielectric sphere in vacuum. As is commonplace for the exterior region, the source potential and the perturbation potential were represented in terms of the standard solutions of the Laplace equation in the spherical coordinate system. A bijective spatial transformation was implemented for the interior region in order to formulate the series representation of the internal potential. Boundary conditions on the spherical surface were enforced and then the orthogonality of tesseral harmonics was employed to derive a transition matrix that relates the expansion coefficients of the perturbation potential in the exterior region to those of the source potential. The angular profile of the perturbation profile changes with distance from the center of the sphere, but eventually it settles down with the perturbation potential decaying as the inverse of the distance squared from the center of the sphere.

Acknowledgement. AL is grateful to the Charles Godfrey Binder Endowment at Penn State for ongoing support of his research activities.

References

- [1] W. R. Smythe, *Static and Dynamic Electricity*, 2nd ed., (New York, NY, USA, McGraw–Hill 1950).
- [2] J. D. Jackson, *Classical Electrodynamics*, 3rd ed., (Hoboken, NJ, USA, Wiley 1999).
- [3] J. I. Gersten and F. W. Smith, *The Physics and Chemistry of Materials*, (New Ork, NY, USA, Wiley 2001).
- [4] J. F. Nye, *Physical Properties of Crystals: Their Representation by Tensors and Matrices*, (Oxford, United Kingdom, Oxford University Press 1985).
- [5] O. D. Kellogg, *Foundations of Potential Theory*, (New York, NY, USA, Dover 1953).
- [6] W. E. Williams, Some boundary value problems in potential theory, *The Quarterly Journal of Mechanics and Applied Mathematics* **14**, (1961) 443–452.
- [7] J. D. Love, Dielectric sphere-sphere and sphere-plane problems in electrostatics, *The Quarterly Journal of Mechanics and Applied Mathematics* **28**, (1975) 449–471.
- [8] D. S. Jones, The scattering of long electromagnetic waves, *The Quarterly Journal of Mechanics and Applied Mathematics* **33**, (1980) 105–122.
- [9] I. V. Lindell, Electrostatic image theory for the dielectric sphere, *Radio Science* **27**, (1992) 1–8.
- [10] M. R. A Majić, B. Auguie, and E. C. Le Ru, Laplace’s equation for a point source near a sphere: improved internal solution using spheroidal harmonics, *IMA Journal of Applied Mathematics* **83**, (2018) 895–907.
- [11] V. L. Sukhorukov, G. Meedt, M. Kürschner, and U. Zimmermann, A single-shell model for biological cells extended to account for the dielectric anisotropy of the plasma membrane, *Journal of Electrostatics* **50**, (2001) 191–204.
- [12] K. Woepfel, Q. Yanga, and X. T. Cui, Recent advances in neural electrode–tissue interfaces, *Current Opinion in Biomedical Engineering* **4**, (2017) 21–31.
- [13] J. C. Everts, B. Senyuk, H. Munder, M. Ravnik, and I. I. Smalyukh, Anisotropic electrostatic screening of charged colloids in nematic solvents, *Science Advances* **7**, (2021) eabd0662.
- [14] J. Plog, Y. Jiang, Y. Pan, and A. L. Yarin, Electrostatic charging and deflection of droplets for drop-on-demand 3D printing within confinements, *Additive Manufacturing* **36**, (2020) 101400.
- [15] D. Medková, *The Laplace Equation: Boundary Value Problems on Bounded and Unbounded Lipschitz Domains*, (Cham, Switzerland, Springer 2018).

- [16] P. Moon and D. E. Spencer, *Field Theory Handbook: Including Coordinate Systems, Differential Equations and Their Solutions*, 2nd ed., (Berlin, Germany, Springer 1971).
- [17] B. A. Auld, *Acoustic Fields and Waves in Solids, Vol. I*, 2nd ed., (Malabar, FL, USA, Krieger 1990).
- [18] A. Charnow and E. Charnow, Fields for which the principal axis theorem is valid, *Mathematical Magazine* **59**, (1986) 222–225.
- [19] G. Strang, *Introduction to Linear Algebra*, 5th ed., (Wellesley, MA, USA, Wellesley–Cambridge 2016).
- [20] T. G. Mackay and A. Lakhtakia, *Modern Analytical Electromagnetic Homogenization with Mathematics*, 2nd ed. (Bristol, United Kingdom, IoP 2020).
- [21] H. Lütkepohl, *Handbook of Matrices* (Chicester, United Kingdom, Wiley 1996).
- [22] P. M. Morse and H. Feshbach, *Methods of Theoretical Physics*, Vol. II (New York, NY, USA, McGraw–Hill 1953), pp. 1920–1921.
- [23] H. M. Alkhoori, A. Lakhtakia, J. K. Breakall, and C. F. Bohren, Plane-wave scattering by an ellipsoid composed of an orthorhombic dielectric–magnetic material, *Journal of the Optical Society of America A* **35**, (2018) 1549–1559.
- [24] N. L. Tsitsas and P. A. Martin, Finding a source inside a sphere, *Inverse Problems* **28**, (2012) 015003.
- [25] J. A. Stratton, *Electromagnetic Theory* (New York, NY, USA, McGraw–Hill 1941).
- [26] J. R. Zurita-Sánchez, Quasi-static electromagnetic fields created by an electric dipole in the vicinity of a dielectric sphere: method of images, *Revista Mexicana de Física* **55**, (2009) 443–449.